Physics and Imaging in Radiation Oncology 16 (2020) 33–36

Contents lists available at ScienceDirect

Physics and Imaging in Radiation Oncology

journal homepage: www.sciencedirect.com/journal/physics-and-imaging-in-radiation-oncology

Technical Note

Measuring eye deformation between planning and proton beam therapy position using magnetic resonance imaging

Myriam G. Jaarsma-Coes [a,b,*], Marina Marinkovic [a], Eleftheria Astreinidou [c], Megan S. Schuurmans [b], Femke P. Peters [c], Gregorius P.M. Luyten [a], Coen R.N. Rasch [c], Jan-Willem M. Beenakker [a,b]

[a] Ophthalmology, Leiden University Medical Centre, Leiden, Netherlands
[b] Radiology, C.J. Gorter Centre for High Field MRI, Leiden University Medical Centre, Leiden, Netherlands
[c] Radiotherapy, Leiden University Medical Centre, Leiden, Netherlands

ARTICLE INFO

Keywords:
Gravity
Eye deformation
MRI
Therapy planning
Uveal melanoma
Ocular imaging

ABSTRACT

Proton beam therapy (PBT) for uveal melanoma (UM) is performed in sitting position, while the acquisition of the Magnetic resonance (MR)-images for treatment planning is performed in supine position. We assessed the effect of this difference in position on the eye- and tumour- shape. Seven subjects and six UM-patients were scanned in supine and a seating mimicking position. The distances between the tumour/sclera in both positions were calculated. The median distance between both positions was 0.1 mm. Change in gravity direction produced no substantial changes in sclera and tumour shape, indicating that supinely acquired MR-images can be used to plan ocular-PBT.

1. Introduction

Uveal melanoma (UM) is the most common primary intraocular tumour, occurring at a rate of approximately 6 cases per million person-years [1,2]. The management of localized UM can be divided into globe-preserving therapy and enucleation, i.e. surgical removal of the eye. The three most common globe-preserving therapies are plaque brachytherapy, stereotactic radiosurgery (SRS) and proton beam therapy (PBT). The optimal treatment modality depends on several factors including size and location of the tumour, proximity to the optic disc or fovea, and patients' preference [3–5].

For larger tumours as well as tumours in close proximity to the optic nerve, stereotactic radiosurgery (SRS) or PBT is generally used. The latter has a dose distribution superior to SRS, allowing sharper dose gradients and highly conformal dose to the tumour, sparing more healthy tissue. As a consequence, PBT potentially provides better clinical outcomes in terms of vision, radiation induced side-effects and eye retention [6–8].

PBT treatment is currently on a generic model of the eye and tumour, based on X-rays, fundus photographs and ocular ultrasound data [6,9] yielding only a rudimentary representation. Magnetic resonance imaging (MRI) however, can be used to construct detailed patient-specific models [10–12]. It is recognized that these models might provide a more accurate representation of the tumour and organs at risk. However, as MRI scans are performed with the patient in prone position and PBT is performed with the patients in "seated" position, the change in gravity direction might induce a geometric mismatch in tumour and/or eye shape between both postures. We therefore, assessed the effect of body pose on the eye- and tumour- shape.

2. Materials and methods

This study was carried out according to the Declaration of Helsinki for experiments involving humans and in accordance with the recommendations of the local Ethic Committee (CME LUMC, Leiden University Medical Centre).

2.1. Subject description

We assessed the effect of body pose on ocular shape in seven healthy subjects and its effect on tumour shape in six UM patients. Eye and tumour shape were compared between sitting up, as during PBT, (flexed) and scanning (supine) position. Additionally, two healthy subjects were scanned to assess the reproducibility of the method. The six

* Corresponding author at: Leiden University Medical Center, P.O. 9600, 2300 RC Leiden, The Netherlands.
E-mail address: m.g.jaarsma@lumc.nl (M.G. Jaarsma-Coes).

https://doi.org/10.1016/j.phro.2020.09.010
Received 20 May 2020; Received in revised form 4 June 2020; Accepted 25 September 2020
Available online 6 October 2020

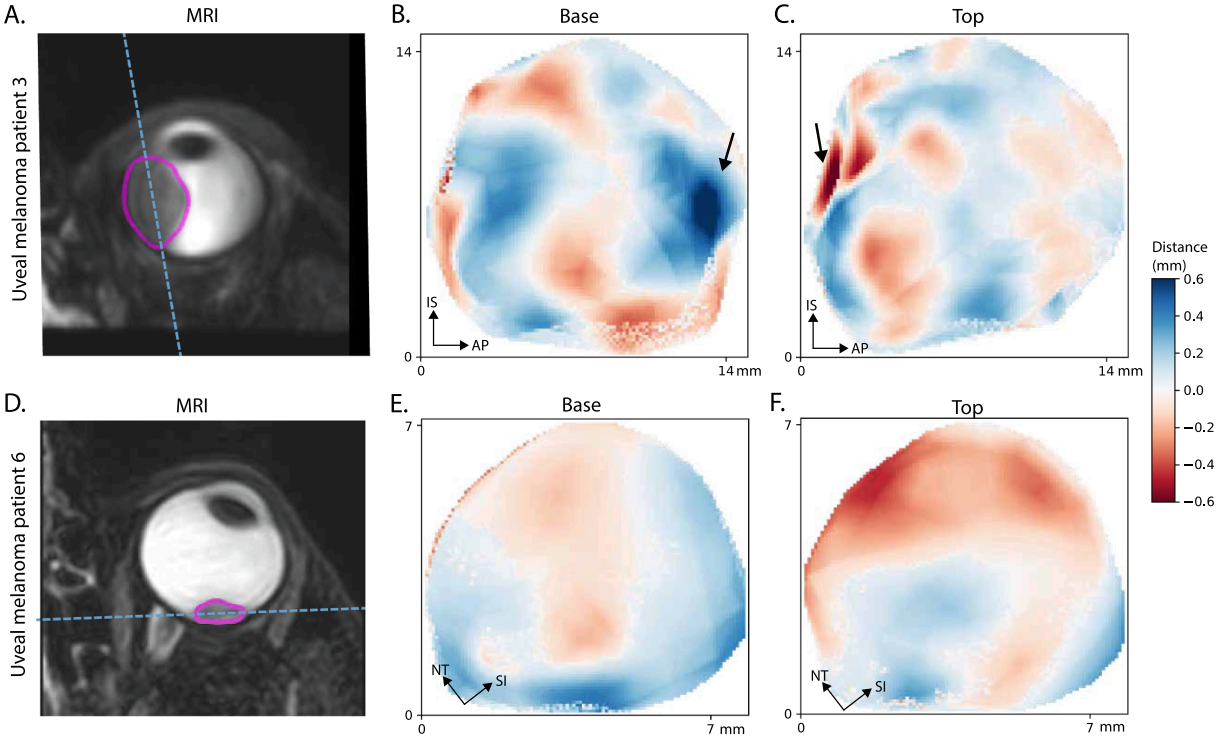

Fig. 1. The measured distances of the tumours of patients 3 and 6. The two regions with outliers (arrow in 1b and 1c) are located near the tumour base and next to a retinal detachment or lens, making segmentation more challenging.

included patients represent the wide variety of tumours that can occur in UM patients. The size of tumours ranged from small (height ≤3 mm) to large (height >8 mm) at time of scanning and differed in composition from mostly melanotic, partially melanotic to amelanotic lesions (supplementary Table 1).

When scanning patients we noticed a deterioration in image quality, especially for the scans acquired in flexed position. Therefore, an additional reproducibility measurement was performed by scanning a patient twice in flexed position and another patient twice in supine position to assess the effect of motion blurring on the determined shape difference.

2.2. MRI setup

All subjects were scanned in a wide bore 3 T MRI (Ingenia, Philips Healthcare, Best, The Netherlands) with one or two 47 mm Rx-surface coils (Philips Healthcare) after giving written informed consent. These coils were mounted on to a flexible eye mask. The limited size of the magnet bore refrained from scanning subjects in sitting position, as during PBT. Therefore the subjects were scanned in a posture that mimics gravity in sitting posture. This was achieved by positioning the subjects on their backs with their chin on the chest. The head was supported to limit head motion during the scans (supplementary Fig. 1c).

For the scans in supine position, the coils were positioned in front of both eyes, which is the optimal location for ocular MRI [13,14]. For the flexed position, however, this configuration is not suitable, as the main direction of the magnetic flux of the surface coil would be parallel to main magnetic field, resulting in no MR-signal. Hence, the coils were positioned to the side of both eyes for imaging in flexed position. In healthy subjects two coils were used, one in front of each eye, in contrast to patients were only one Rx-surface coil, in front of the affected eye, was used in accordance with the current clinical protocol [15]. A schematic representation of the two positions in the MRI scanner with coil positions is shown in supplementary Fig. 1a.

Healthy subjects were scanned in a dedicated session for this study with a protocol consisting of a survey to plan the subsequent T2-weighted scans (TR:2500 ms/TE:285 ms/Voxel size:(0.9 mm)^3 /Scan time:3:13 min) in both flexed and supine position. For the patients, additional scans were added at the end of the clinical protocol consisting of a survey with subsequent T2-weighted scan (TR:2500 ms/TE:293 ms/Voxel size:(0.8 mm)^3/Scan time:3:35 min) in flexed position. A detailed description of the scan parameters can be found in supplementary Table 2.

2.3. Analysis

To compare the eye and tumour shape between both postures, the MR-images were registered and the anatomies segmented. First the sclera in supine position was segmented to obtain a mask for registration. Subsequently the flexed image was registered to the supine image. Finally, the sclera, lens and if appropriate tumour were segmented on both images.

Registration of the eyes was challenging as not only the complete head was in different positions between both scans, but the eyes can, additionally, rotate within the head. Hence, a masked registration, in which the anatomy outside the eye is discarded, was performed. Registration was performed using Elastix 4.9.0 [16] in Mevislab 3.0.2 (MeVis Medical Solutions AG, Bremen, Germany) [17]. The eye mask used in the registration was created by segmenting the sclera in the supinely acquired scan. This segmentation was subsequently extended by 2.5 mm to include the optic nerve as an additional registration landmark. The MRIs in flexed position were registered to the supinely acquired scans using the obtained mask. If necessary, additional manual registration correction was performed in MeVisLab.

After registration, the sclera, lens and tumour were segmented using Subdivision Surfaces controlled by the maximal gradient magnitude [18]. This method is independent of signal amplitude which varied per MRI scan, especially because of the different coil positions between supine and flexed acquisitions. When needed, manual corrections were made in the segmentation.

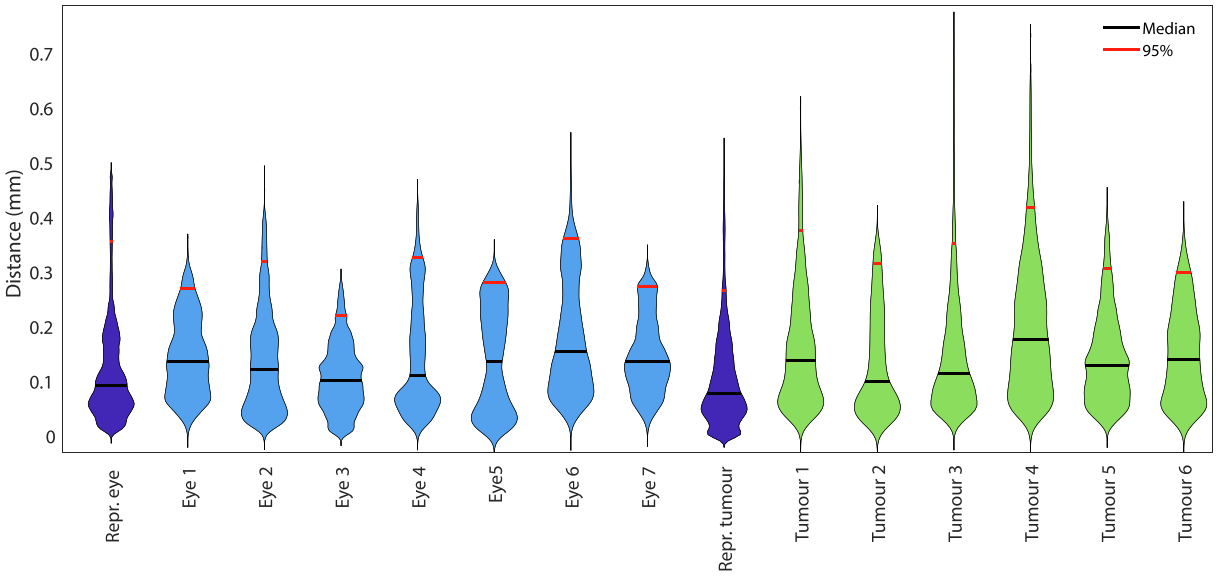

Fig. 2. Violin plots showing the distribution of the measured distances between supine and flexed position.

The difference in shape of the eye and tumour between both postures were afterwards determined by calculating the distance, i.e. for each mesh point of the supine position the closest mesh point in the flexed position, as a measure for the shape difference. For the eye-shape, points anterior from the lens were discarded as susceptibility artefacts often occur at the air-tissue interface of the cornea. The segmented mesh was subdivided into edges with a length less than 0.16 mm resulting in approximately 10^5 points for the healthy eyes and $>10^4$ points describing the tumour boundaries. Finally the concordance index [19] was calculated.

3. Results

All flexed images were successfully registered to the supine images in the seven healthy subjects and six patients, although most registrations needed additional manual (rigid) registration correction. A detailed description can be found in the supplementary materials. The average 95th percentile reproducibility in the two healthy volunteers and two patients was 0.3 mm.

In healthy subjects the median measured distances between the eye in supine and flexed position was 0.1 mm with a 95th percentile of 0.3 mm with a maximum of 0.4 mm. The concordance index for all eyes was 0.95 or higher and the volume change was less than 0.6%. A deformation map of all healthy eyes can be found in supplementary Fig. 1.

In tumours of the patients an average median distance between both postures of 0.1 mm was found with an 95th percentile of 0.3 mm with a maximum of 0.4 mm, Fig. 2. Although tThe distances were in generally very similar to the healthy subjects, some local regions showed distances $>$ 0.4 mm, for example in patient 3 (Fig. 1 b and c). These outlier regions were mostly caused by motion artefacts in one of the two scans. The concordance index of the tumours ranged from 0.85 to 0.95.

An overview of the results for all the subjects can be found in supplementary Table 4.

4. Discussion

MRI based PBT treatment planning systems rely on data obtained while the patient is in supine position whereas PBT is performed in seated position, raising the question whether the effect of gravity on the shape of the eye and tumour should be taken into account in these models. In this study we assessed the effect of body pose on ocular shape in seven healthy subjects and six UM patients using MRI. We showed that in healthy subjects the eye shape changes less than 0.4 mm which is close to the measured reproducibility of 0.3 mm and well within our measured isotropic voxel size of 0.9 mm. This indicates that the eyes retains its shape even when gravity works in a different direction. Similarly, the median shape change for the tumours was 0.1 mm with a maximum 95th percentile of 0.4 mm which was in line with the reproducibility of 0.3 mm and well within voxel limit.

Slopsema et al. [20] showed that the shape change of the eye due to gravity is less than 0.6 $\pm$ 0.3 mm, by comparing the tantalum clip positions on supinely acquired CT images, with clip positions obtained from a geometrical eye-model based on orthogonal X-rays acquired in sitting position. As this observed difference is probably largely the result of uncertainties in the geometrical eye-model used for PBT planning, such as the rotational center of the eye, the actual change in eye shape is expected to be less than the observed differences between the CT-based and X-ray based eye-model. These results are therefore in line with this study as we show that the potential shape change of the eye due to gravity is $<$0.4 mm.

When comparing the distance measurements of the eyes and tumours in different positions we observed some local outliers ($>$0.4 mm) in the tumour distance measurements. This is likely caused by the fact that tumour segmentation is more challenging than eye segmentation. For the eye segmentation the vitreous-sclera boundary has a high contrast where for tumour segmentation the tumour is not only located next to the vitreous but also often in close proximity of the lens or retinal detachment. These structures have a much lower contrast with the tumour. Furthermore, more motion artefacts were present in the scans of the patients as we scanned them in the flexed position at the end of a longer protocol. These outliers likely explain the lower concordances indexes (0.85–0.95 vs $>$0.95) we measured. Furthermore, the lower concordance indexes were observed in the smallest lesions, suggesting that the tumour size might be the biggest contributing factor as a small absolute change has a large effect on the concordances index of small lesions. The small distance measurements between both postures, which were less than 0.3 mm, are therefore a good confirmation that the change in tumour shape was very small.

These are important result as MRI is more and more used for diagnosis and follow up of uveal melanoma patients and more and more PBT treatment centres and companies are working on improvement of treatment planning systems for uveal melanoma based on MRI, or CT which are also acquired in supine position [10,21]. The maximum eye and tumour deformation measured was lower than 0.6 mm, the

interobserver variability of ultrasound in the evaluation of uveal melanoma thickness as determined in a comprehensive study by Char et al. [22]. It was also in the same order as eye movement during PBT treatment (average of 0.4–0.9 mm) [23]. Furthermore, any potential effect of gravity on the shape of the eye was well within the safety margin of 2–3 mm currently used for PBT planning of UM [24,25].

One of the limitations of our study was the small number of patients included in this study, which was primarily limited due to the burden of additional scanning in flexed position. Nonetheless, all different shapes (dome, mushroom), sizes (small, medium, large) and compositions (melanotic, partially melanotic and amelanotic) tumours were represented in the study population. As in none of these patients a significant tumour deformation was detected, we are confident that these findings are valid for the general population of UM patients. Furthermore, our measurement of deformation was limited by the voxel size of the 3D MRI acquisition. However, using interpolation and information of neighbouring voxels, we were able to estimate the edge location with subvoxel accuracy, as was confirmed by the reproducibility of 0.3 mm.

In conclusion, changes in gravity direction produce no substantial changes in sclera and tumour shape. Our results indicate that supinely acquired MR images can be used to accurately plan ocular PBT, which is performed in sitting position.

Declaration of Competing Interest

The authors declare that they have no known competing financial interests or personal relationships that could have appeared to influence the work reported in this paper.

Acknowledgements

The authors thank Kilany Hassan and Berend Stoel (LKEB, LUMC) fort their help with image registration. Part of this work is performed within the research program PROTONS4vision with project number 14654 which is financed by the Netherlands Organization for Scientific Research (NWO).

Appendix A. Supplementary data

Supplementary data to this article can be found online at https://doi.org/10.1016/j.phro.2020.09.010.

References

[1] Singh AD, Turell ME, Topham AK. Uveal melanoma: Trends in incidence, treatment, and survival. Ophthalmology 2011;118:1881–5. https://doi.org/10.1016/j.ophtha.2011.01.040.
[2] Chang AE, Karnell LH, Menck HR. The national cancer data base report on cutaneous and noncutaneous melanoma: A summary of 84,836 cases from the past decade. Cancer 1998;83:1664–78. https://doi.org/10.1002/(SICI)1097-0142(19981015)83:8<1664::AID-CNCR23>3.0.CO;2-G.
[3] Krantz BA, Dave N, Komatsubara KM, Marr BP, Carvajal RD. Uveal melanoma: epidemiology, etiology, and treatment of primary disease. Clin Ophthalmol 2017;11:279. https://doi.org/10.2147/OPTH.S89591.
[4] Blum ES, Yang J, Komatsubara KM, Carvajal RD. Clinical Management of Uveal and Conjunctival Melanoma. Oncology (Williston Park) 2016;30(1):29–43.
[5] Koopmans AE, de Klein A, Naus NC, Kilic E. Diagnosis and Management of Uveal Melanoma. Eur Ophthalmic Rev 2013.
[6] Sikuade MJ, Salvi S, Rundle PA, Errington DG, Kacperek A, Rennie IG. Outcomes of treatment with stereotactic radiosurgery or proton beam therapy for choroidal melanoma. Eye (Lond) 2015;29:1194–8. https://doi.org/10.1038/eye.2015.109.
[7] Egger E, Zografos L, Schalenbourg A, Beati D, Böhringer T, Chamot L, et al. Eye retention after proton beam radiotherapy for uveal melanoma. Int J Radiat Oncol Biol Phys 2003;55:867–80. https://doi.org/10.1016/S0360-3016(02)04200-1.
[8] Verma V, Mehta MP. Clinical Outcomes of Proton Radiotherapy for Uveal Melanoma. Clin Oncol 2016;28:e17–27. https://doi.org/10.1016/j.clon.2016.01.034.
[9] Aziz S, Taylor A, McConnachie A, Kacperek A, Kemp E. Proton beam radiotherapy in the management of uveal melanoma: Clinical experience in Scotland. Clin Ophthalmol 2009;3:49–55.
[10] Nguyen HG, Sznitman R, Maeder P, Schalenbourg A, Peroni M, Hrbacek J, et al. Personalized Anatomic Eye Model From T1-Weighted Volume Interpolated Gradient Echo Magnetic Resonance Imaging of Patients With Uveal Melanoma. Int J Radiat Oncol Biol Phys 2018;102:813–20. https://doi.org/10.1016/j.ijrobp.2018.05.004.
[11] Fleury E, Trnková P, Erdal E, Hassan K, Beenakker J, Herault J, et al. OC-669 Development of a novel MRI-only treatment planning approach for ocular proton therapy. Radiother Oncol 2019;133:S350–1. https://doi.org/10.1016/s0167-8140(19)31089-8.
[12] Beenakker JWM, Hassan MK, Shamonin D, Shahzad R, Webb AG, Stoel B, et al. Automated analysis of eye tumor MR-images for an improved treatment determination. Acta Ophthalmol 2018;96:11–2. https://doi.org/10.1111/aos.13972_34.
[13] Beenakker JWM, Ferreira TA, Soemarwoto KP, Genders SW, Teeuwisse WM, Webb AG, et al. Clinical evaluation of ultra-high-field MRI for three-dimensional visualisation of tumour size in uveal melanoma patients, with direct relevance to treatment planning. Magn Reson Mater Physics, Biol Med 2016;29:571–7. https://doi.org/10.1007/s10334-016-0529-4.
[14] De Graaf P, Göricke S, Rodjan F, Galluzzi P, Maeder P, Castelijns JA, et al. Guidelines for imaging retinoblastoma: Imaging principles and MRI standardization. Pediatr Radiol 2012;42:2–14. https://doi.org/10.1007/s00247-011-2201-5.
[15] Ferreira TA, Fonk LG, Jaarsma-Coes MG, van Haren GGR, Marinkovic M, Beenakker JWM. MRI of uveal melanoma. Cancers (Basel) 2019;11:1–20. https://doi.org/10.3390/cancers11030377.
[16] Klein S, Staring M, Murphy K, Viergever MA, Pluim JPW. Elastix: A toolbox for intensity-based medical image registration. IEEE Trans Med Imaging 2010;29:196–205. https://doi.org/10.1109/TMI.2009.2035616.
[17] Ritter F, Boskamp T, Homeyer A, Laue H, Schwier M, Link F, et al. Medical Image Analysis: A Visual Approach. IEEE Pulse 2011;2:60–70. https://doi.org/10.1109/MPUL.2011.942929.
[18] Kitslaar PH, van't Klooster R, Staring M, Lelieveldt BPF, van der Geest RJ. Segmentation of branching vascular structures using adaptive subdivision surface fitting. Proc. SPIE 9413, Medical Imaging 2015: Image Processing, 94133Z (20 March 2015); https://doi.org/10.1117/12.2082222.
[19] Hanna GG, Hounsell AR, O'Sullivan JM. Geometrical Analysis of Radiotherapy Target Volume Delineation: A Systematic Review of Reported Comparison Methods. Clin Oncol 2010;22(7):515–25. https://doi.org/10.1016/j.clon.2010.05.006.
[20] Slopsema RL, Mamalui M, Bolling J, Flampouri S, Yeung D, Li Z, et al. Can CT imaging improve targeting accuracy in clip-based proton therapy of ocular melanoma? Phys Med Biol 2019;64(3):035010. https://doi.org/10.1088/1361-6560/aaf9c9.
[21] Hrbacek J, Mishra KK, Kacperek A, Dendale R, Nauraye C, Auger M, et al. Practice Patterns Analysis of Ocular Proton Therapy Centers: The International OPTIC Survey. Int J Radiat Oncol Biol Phys 2016;95:336–43. https://doi.org/10.1016/j.ijrobp.2016.01.040.
[22] Char DH, Kroll S, Stone RD, Harrie R, Kerman B. Ultrasonographic measurement of uveal melanoma thickness: Interobserver variability. Br J Ophthalmol 1990;74(3):183–5. https://doi.org/10.1136/bjo.74.3.183.
[23] Shin D, Yoo SH, Moon SH, Yoon M, Lee SB, Park SY. Eye tracking and gating system for proton therapy of orbital tumors. Med Phys 2012; 39.7 Part1:4265–73. https://doi.org/10.1118/1.4729708.
[24] Dendale R, Lumbroso-Le Rouic L, Noel G, Feuvret L, Levy C, Delacroix S, et al. Proton beam radiotherapy for uveal melanoma: Results of Curie Institut-Orsay Proton Therapy Center (ICPO). Int J Radiat Oncol Biol Phys 2006;65(3):780–7. https://doi.org/10.1016/j.ijrobp.2006.01.020.
[25] Damato B, Kacperek A, Chopra M, Campbell IR, Errington RD. Proton beam radiotherapy of choroidal melanoma: The Liverpool-Clatterbridge experience. Int J Radiat Oncol Biol Phys 2005;62(5):1405–11. https://doi.org/10.1016/j.ijrobp.2005.01.016.